Journal of Sound and Vibration 329 (2010) 425–442

Contents lists available at ScienceDirect

Journal of Sound and Vibration

journal homepage: www.elsevier.com/locate/jsvi

Three-dimensional free vibration of thick functionally graded annular plates in thermal environment

P. Malekzadeh [a,b,*], S.A. Shahpari [c], H.R. Ziaee [d]

[a] Department of Mechanical Engineering, Persian Gulf University, Bushehr 75168, Iran
[b] Center of Excellence for Computational Mechanics, Shiraz University, Shiraz, Iran
[c] Engineering Research Institute, Tehran, Iran
[d] Department of Mechanical Engineering, Azad University, Shiraz, Iran

ARTICLE INFO

Article history:
Received 23 January 2009
Received in revised form
18 September 2009
Accepted 19 September 2009
Handling Editor: A.V. Metrikine
Available online 9 October 2009

ABSTRACT

The free vibration analysis of functionally graded (FG) thick annular plates subjected to thermal environment is studied based on the 3D elasticity theory. The material properties are assumed to be temperature dependent and graded in the thickness direction. Considering the thermal environment effects and using Hamilton's principle, the equations of motion are derived. The effects of the initial thermal stresses are considered accurately by obtaining them from the 3D thermoelastic equilibrium equations. The differential quadrature method (DQM) as an efficient and accurate numerical tool is used to solve both the thermoelastic equilibrium and free vibration equations. Very fast rate of convergence of the method is demonstrated. Also, the formulation is validated by comparing the results with those obtained based on the first-order shear deformation theory and also with those available in the literature for the limit cases, i.e. annular plates without thermal effects. The effects of temperature rise, material and geometrical parameters on the natural frequencies are investigated. The new results can be used as benchmark solutions for future researches.

© 2009 Elsevier Ltd. All rights reserved.

1. Introduction

Functionally graded materials (FGMs) are special composite whose thermo-mechanical properties have smooth and continuous spatial variation due to a continuous change in composition, in morphology, in microstructure, or in crystal structure. FGMs posses various advantages over the conventional composite laminates, such as smaller thermal stresses, stress concentrations, attenuation of stress waves, etc. Therefore, FGMs have received wide applications as structural components in modern industries such as mechanical, aerospace, nuclear, reactors, and civil engineering.

The structural elements made of FGMs work often in thermal environment with high temperature which induce large thermoelastic stresses and consequently change the mechanical behavior of these materials. Hence, the study of vibration characteristic of these types of material under thermal conditions is of great interest for engineering design and manufacture.

Compared with the free vibration analysis of FG beams and rectangular plates (see for example [1–12]), the studies concerned with the free vibration of FG circular and annular plates is very limited in number and are discussed briefly here. Eraslan and Akis [13] obtained the closed-form solution for functionally graded rotating solid shaft and rotating solid disk

* Corresponding author at: Department of Mechanical Engineering, Persian Gulf University, Bushehr 75168, Iran. Tel.: +98 771 4222150; fax: +98 771 4540376.
E-mail addresses: p_malekz@yahoo.com, malekzadeh@pgu.ac.ir (P. Malekzadeh).

0022-460X/$ - see front matter © 2009 Elsevier Ltd. All rights reserved.
doi:10.1016/j.jsv.2009.09.025

under generalized plane strain and plane stress assumptions, respectively. Prakash and Ganapathi [14] analyzed the asymmetric flexural vibration and thermoelastic stability of FGMs circular plates based on the first-order shear deformation theory (FSDT) using the finite element method. Efraim and Eisenberger [15] presented the vibration analysis of annular plates with variable thickness made of isotropic material and FGMs by the exact element method. They used the FSDT to formulate the problem. Nie and Zhong [16] investigated the three-dimensional vibration of functionally graded circular plates using a semi-analytical method based on the state space method and DQM. They used the state space method and the DQM to discretize the equations of motion in the thickness and the radial directions, respectively. Dong [17] studied the three-dimensional free vibration of functionally graded circular and annular plates using the Chebyshev–Ritz method. Recently, Zhao et al. [18] presented a free vibration analysis of functionally graded plates using the element-free kp-Ritz method and based on the first-order shear deformation plate theory. But the circular and annular plates were not investigated. Also, in these works only the mechanical vibrations were investigated carefully and the effects of initial stresses due to thermal environment were not considered. Kumar et al. [19] carried out the acoustic response of the functionally graded material elliptic disc. Displacement, velocity, acceleration, radiated sound pressure, radiated sound power level and radiation efficiency of the elliptic disc were examined over a range of varying frequencies.

The differential quadrature method (DQM) is found to be a simple and efficient numerical technique for structural analysis [2,12,18–21]. Better convergence behavior is observed by DQM compared with its peer numerical competent techniques viz. the finite element method, the finite difference method, the boundary element method and the meshless technique.

To the authors' best knowledge, in the previous works only the mechanical vibrations of FG circular and annular plates are investigated and the effects of thermal environment are not considered. Hence, in this paper the three-dimensional free vibration of FG circular and annular plates with arbitrary boundary conditions and under thermal environment are studied. The material properties are assumed to be temperature dependent and graded in the thickness direction, which can vary according to power law distributions in terms of the volume fractions of the constituents, exponentially or any other formulations in this direction. The initial thermal stresses in the plate due to the temperature rise are accurately determined by solving the three-dimensional thermoelastic equilibrium equations. Both the thermoelastic equilibrium equations as well as the equations of motion, subjected to the related boundary conditions, are solved by using the differential quadrature method (DQM) [2,12,20–23]. Specially using the DQM along the graded direction enables one to accurately and efficiently discretize the variable coefficient partial differential equations in this direction and implement the boundary conditions in their strong forms. The accuracy and convergence of the present method are demonstrated through numerical results. Finally, parametric study is carried out to highlight the influences of uniform and non-uniform temperature rise, boundary conditions, dependence of material properties on temperature and material property graded indexes on the vibration frequencies of FG thick annular plates in thermal environment.

2. Governing equations

Consider a thick FG annular plate as shown in Fig. 1. A cylindrical coordinate system (r, θ, z) is used to label the material point of the plate in the unstressed reference configuration. The displacement components of an arbitrary material point of the plate are denoted as u, v and w in the r, θ and z-directions, respectively.

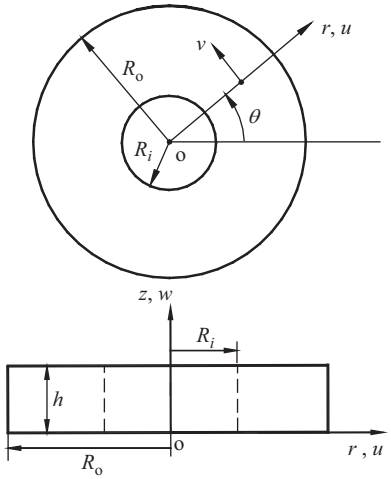

Fig. 1. Geometry and coordinate system of the FG annular plates.

2.1. FGMs relations

The material properties of the plate are assumed to vary continuously through the thickness of the plate, i.e. in the z-direction. The material properties are assumed to vary according to power law distribution in terms of the volume fractions of the constituents or exponentially through the thickness. In the first case, the material composition continuously varies such that the surface z=h is ceramic-rich, whereas the surface z=0 is metal-rich. Based on the power law distribution, a typical effective material property 'P' of the FG plate is obtained as [11]

$$P(z,T) = P_m(T) + [P_c(T) - P_m(T)]\left(\frac{z}{h}\right)^p, \tag{1}$$

where subscripts m and c refer to the metal and ceramic constituents, respectively; p is the power law index or the material property graded index; h is the thickness of plate; and T [=$T(z)$] is the temperature (in Kelvin) at an arbitrary material point of the plate.

In the second case, it is assumed that the material properties have the following exponential distributions in the thickness direction of the plates:

$$P(z,T) = P_m(T)\mathrm{e}^{\gamma(z/h)}, \tag{2}$$

where γ is the material property graded index.

For FG plate constituents, i.e. ceramic and metal, the material properties are temperature dependent and a typical property 'Q' of them can be expressed as a function of temperature as [11]

$$Q(T) = Q_0(Q_{-1}T^{-1} + 1 + Q_1T + Q_2T^2 + Q_3T^3). \tag{3}$$

The coefficients Q_i (i=−1, 0, 1, 2) are unique to the constituent materials.

The three-dimensional constitutive relations for a linear elastic orthotropic FG plate including the thermal effects can be written as

$$\begin{Bmatrix} \hat{\sigma}_{rr} \\ \hat{\sigma}_{\theta\theta} \\ \hat{\sigma}_{zz} \\ \hat{\sigma}_{z\theta} \\ \hat{\sigma}_{rz} \\ \hat{\sigma}_{r\theta} \end{Bmatrix} = \begin{bmatrix} C_{11} & C_{12} & C_{13} & 0 & 0 & 0 \\ C_{12} & C_{22} & C_{23} & 0 & 0 & 0 \\ C_{13} & C_{23} & C_{33} & 0 & 0 & 0 \\ 0 & 0 & 0 & C_{44} & 0 & 0 \\ 0 & 0 & 0 & 0 & C_{55} & 0 \\ 0 & 0 & 0 & 0 & 0 & C_{66} \end{bmatrix} \begin{Bmatrix} \hat{\varepsilon}_{rr} - \alpha_1(z,T)\Delta T \\ \hat{\varepsilon}_{\theta\theta} - \alpha_2(z,T)\Delta T \\ \hat{\varepsilon}_{zz} - \alpha_3(z,T)\Delta T \\ 2\hat{\varepsilon}_{z\theta} \\ 2\hat{\varepsilon}_{rz} \\ 2\hat{\varepsilon}_{r\theta} \end{Bmatrix}, \tag{4}$$

where $\hat{\sigma}_{ij}$ and $\hat{\varepsilon}_{ij}$ ($i,j = r,\theta,z$) are the components of stress and strain tensor components, respectively; C_{ij} [= $C_{ij}(z,T)$; i,j = 1, 2, 3] are the material elastic coefficients; $\alpha_i(z,T)$ are the thermal expansion coefficients; ΔT (= $T - T_0$) is the temperature rise and T_0 is the reference temperature at which the plate is stress free. The material elastic coefficients C_{ij} [= $C_{ij}(z,T)$] for an isotropic plate are related to the elastic material properties as follows:

$$C_{11} = C_{22} = C_{33} = \frac{(1-\nu)E}{(1+\nu)(1-2\nu)}, C_{12} = C_{23} = C_{13} = \frac{\nu E}{(1+\nu)(1-2\nu)}, C_{44} = C_{55} = C_{66} = \frac{E}{2(1+\nu)}, \tag{5a–i}$$

where E [=$E(z,T)$]E and ν [= $\nu(z,T)$] are Young's modulus and Poisson's ratio, respectively.

2.2. Thermoelastic equilibrium

In this section, the thermoelastic equilibrium equations based on the three-dimensional elasticity theory for the initial thermal stress evaluation are presented. It is assumed that the plate is stress free at the temperature T_0. Then, if the FG plate operates in a thermal environment, non-uniform temperature rise or uniform temperature rise together with mechanical constraints at its boundaries causes some thermal stresses in it. These stresses affect the vibration characteristic of the plate. In this study, it is assumed that the temperature rise is uniform or varies across the thickness of the plate and no heat generation source exists within the plate. Hence, the temperature distribution along the thickness direction can be obtained by solving the following steady-state one-dimensional heat transfer equation through the thickness of the plate:

$$K(z)\frac{\mathrm{d}^2T}{\mathrm{d}z^2} + \frac{\mathrm{d}K(z)}{\mathrm{d}z}\frac{\mathrm{d}T}{\mathrm{d}z} = 0, \tag{6}$$

where K is the thermal conductivity of the plate. Different thermal boundary conditions can be considered at the top and the bottom surfaces of the plate. Usually, the prescribed temperature at the top and bottom surfaces of FG beams and plates were considered as the thermal boundary conditions in the literature. Hence, for brevity purpose and without loss of

generality, here these type of the boundary conditions are considered, which for plate problem become

$$T = T_m \text{ at } z = 0 \text{ and } T = T_c \text{ at } z = h. \tag{7a, b}$$

For the case of power law distribution, the solution of Eq. (6) subjected to the boundary conditions (7) can be obtained by means of polynomial series solutions. The result is

$$T(z) = T_m + \frac{\Delta T}{C}\left[\left(\frac{2z+h}{2h}\right) - \frac{K_{cm}}{(p+1)K_m}\left(\frac{2z+h}{2h}\right)^{p+1} + \frac{K_{cm}^2}{(2p+1)K_m^2}\left(\frac{2z+h}{2h}\right)^{2p+1} - \frac{K_{cm}^3}{(3p+1)K_m^3}\left(\frac{2z+h}{2h}\right)^{3p+1} + \frac{K_{cm}^4}{(4p+1)K_m^4}\left(\frac{2z+h}{2h}\right)^{4p+1} - \frac{K_{cm}^5}{(5p+1)K_m^5}\left(\frac{2z+h}{2h}\right)^{5p+1}\right], \tag{8}$$

where $K_{cm} = K_c - K_m$ and

$$C = 1 - \frac{K_{cm}}{(p+1)K_m} + \frac{K_{cm}^2}{(2p+1)K_m^2} - \frac{K_{cm}^3}{(3p+1)K_m^3} + \frac{K_{cm}^4}{(4p+1)K_m^4} - \frac{K_{cm}^5}{(5p+1)K_m^5}.$$

Also, for the plates with the exponential distribution of the material properties, the temperature distribution can be easily obtained directly from Eq. (6).

Due to axisymmetric thermal loading, the thermoelastic equilibrium equations in terms of displacement components for a linear elastic FG plate with infinitesimal deformations become δu:

$$C_{11}\frac{\partial^2 u_0}{\partial r^2} + \left(\frac{C_{11}}{r}\right)\frac{\partial u_0}{\partial r} - \left(\frac{C_{11}}{r^2}\right)u_0 + C'_{44}\,\frac{\partial u_0}{\partial z} + C_{44}\frac{\partial^2 u_0}{\partial z^2} + (C_{12}+C_{44})\frac{\partial^2 w_0}{\partial r\,\partial z} + C'_{44}\,\frac{\partial w_0}{\partial r} = 0, \tag{9}$$

δw:

$$(C_{12}+C_{44})\frac{\partial^2 u_0}{\partial z \partial r} + C'_{12}\,\frac{\partial u_0}{\partial r} + \left(\frac{C_{12}+C_{44}}{r}\right)\frac{\partial u_0}{\partial z} + \left(\frac{C'_{12}}{r}\right)u_0 + C_{44}\frac{\partial^2 w_0}{\partial r^2} + \left(\frac{C_{44}}{r}\right)\frac{\partial w_0}{\partial r} + C_{11}\frac{\partial^2 w_0}{\partial z^2} + C'_{11}\,\frac{\partial w_0}{\partial z} = (C'_{12}\ + C'_{12}\ + C'_{11}\ )\alpha\Delta T + (2C_{12}+C_{11})\alpha\frac{\partial(\Delta T)}{\partial z}, \tag{10}$$

where $C'_{ij} = \mathrm{d}C_{ij}/\mathrm{d}z$; u_0 and w_0 are the displacements of an arbitrary material point along the r- and z-directions, respectively. Hereafter, a subscript '0' is used to represent the variables of the deformation field and the stress components in the equilibrium state of the plate in the thermal environment.

The related boundary conditions are as follows:

At the surfaces z=0, h:

$$\sigma_{0zr} = C_{44}\left(\frac{\partial u_0}{\partial z} + \frac{\partial w_0}{\partial r}\right) = 0, \sigma_{0zz} = C_{12}\left(\frac{\partial u_0}{\partial r} + \frac{u_0}{r}\right) + C_{11}\frac{\partial w_0}{\partial z} - (C_{11}+2C_{12})\alpha_1\Delta T = 0. \tag{11a, b}$$

At the surfaces r=R_i and R_o:

$$\text{either } u_0 = 0 \text{ or } \ \sigma_{0rr} = C_{11}\frac{\partial u_0}{\partial r} + C_{12}\left(\frac{u_0}{r} + \frac{\partial w_0}{\partial z}\right) - (C_{11}+2C_{12})\alpha_1\Delta T = 0, \tag{12a, b}$$

$$\text{either } w_0 = 0 \text{ or } \ \sigma_{0rz} = C_{44}\left(\frac{\partial u_0}{\partial z} + \frac{\partial w_0}{\partial r}\right) = 0. \tag{13a, b}$$

Different types of classical boundary conditions at the edges of the plate can be obtained by combining the condition stated in Eqs. (11)–(13). For example, at the edges r=R_i and R_o one has

$$\textit{simply supported}\ (\mathrm{S}): \ \ w_0 = 0, \sigma_{0rr} = C_{11}\frac{\partial u_0}{\partial r} + C_{12}\left(\frac{u_0}{r} + \frac{\partial w_0}{\partial z}\right) - (C_{11}+2C_{12})\alpha_1\Delta T = 0, \tag{14a, b}$$

$$\textit{clamped}\ (\mathrm{C}): \ \ u_0 = 0, w_0 = 0, \tag{15a, b}$$

$$\textit{free}\ (\mathrm{F}): \ \ \sigma_{0rr} = C_{11}\frac{\partial u_0}{\partial r} + C_{12}\left(\frac{u_0}{r} + \frac{\partial w_0}{\partial z}\right) - (C_{11}+2C_{12})\alpha_1\Delta T = 0, \sigma_{0rz} = C_{44}\left(\frac{\partial u_0}{\partial z} + \frac{\partial w_0}{\partial r}\right) = 0. \tag{16a, b}$$

2.3. Vibration analysis

To study the free vibration characteristic of the plate in the thermal environment, the displacement components of an arbitrary material point (r, θ, z) are perturbed around its equilibrium position in thermal environment. Hence, the total

displacement components measured from the plate undeformed configurations become

$$\hat{u}(r,\theta,z,t) = u_0(r,z) + u(r,\theta,z,t), \hat{v}(r,\theta,z,t) = v_0(r,z) + v(r,\theta,z,t) = v(r,\theta,z,t), \hat{w}(r,\theta,z,t) = w_0(r,z) + w(r,\theta,z,t), \tag{17a–c}$$

where $\hat{u}$, $\hat{v}$ and $\hat{w}$ are the total displacement components along the r-, θ- and z-directions, respectively.

The free vibration equations of motion with the related boundary conditions can be obtained by using Hamilton's principle, which has the following form:

$$\int_{t_1}^{t_2} (\delta K - \delta U)\,\mathrm{d}t = 0, \tag{18}$$

where K and U are the kinetic and the potential energy of the plate; t_1 and t_2 are two arbitrary values of time. The virtual work of the internal forces, including the initial thermal stresses, can be obtained from the variation of the plate elastic potential energy, which is

$$\delta U = \int_{R_i}^{R_o}\int_0^{2\pi}\int_{-h/2}^{h/2} [(\sigma_{rr}+\sigma_{0rr})\delta\hat{\varepsilon}_{rr} + (\sigma_{\theta\theta}+\sigma_{0\theta\theta})\delta\hat{\varepsilon}_{\theta\theta} + (\sigma_{zz}+\sigma_{0rz})\delta\hat{\varepsilon}_{zz} + 2(\sigma_{rz}+\sigma_{0rz})\delta\hat{\varepsilon}_{rz} + 2\sigma_{r\theta}\delta\hat{\varepsilon}_{r\theta} + 2\sigma_{\theta z}\delta\hat{\varepsilon}_{\theta z}]r\,\mathrm{d}\theta\,\mathrm{d}r\,\mathrm{d}z, \tag{19}$$

where σ_{ij} $(i,j = r,\theta,z)$ are that parts of the total stress tensor $\hat{\sigma}_{ij}$ which are due to vibratory motion.

To include the effects of the initial thermal stresses in the equations of motion, the nonlinear terms in the strain–displacement relations of vibration should be considered:

$$\hat{\varepsilon}_{rr} = \frac{\partial\hat{u}}{\partial r} + \frac{1}{2}\left[\left(\frac{\partial\hat{u}}{\partial r}\right)^2 + \left(\frac{\partial\hat{v}}{\partial r}\right)^2 + \left(\frac{\partial\hat{w}}{\partial r}\right)^2\right], \tag{20a}$$

$$\hat{\varepsilon}_{\theta\theta} = \frac{1}{r}\left(\frac{\partial\hat{v}}{\partial\theta} + \hat{u}\right) + \frac{1}{2r^2}\left[\left(\frac{\partial\hat{u}}{\partial\theta} - \hat{v}\right)^2 + \left(\frac{\partial\hat{v}}{\partial\theta} + \hat{u}\right)^2 + \left(\frac{\partial\hat{w}}{\partial\theta}\right)^2\right], \tag{20b}$$

$$2\hat{\varepsilon}_{r\theta} = \frac{\partial\hat{v}}{\partial r} + \frac{1}{r}\left(\frac{\partial\hat{u}}{\partial\theta} - \hat{v}\right) + \frac{1}{r}\left[\frac{\partial\hat{u}}{\partial r}\left(\frac{\partial\hat{u}}{\partial\theta} - \hat{v}\right) + \frac{\partial\hat{v}}{\partial r}\left(\frac{\partial\hat{v}}{\partial\theta} + \hat{u}\right) + \hat{u}\left(\frac{\partial\hat{v}}{\partial r}\right) + \frac{\partial\hat{w}}{\partial r}\frac{\partial\hat{w}}{\partial\theta}\right], \tag{20c}$$

$$2\hat{\varepsilon}_{\theta z} = \frac{\partial\hat{v}}{\partial z} + \frac{1}{r}\frac{\partial\hat{w}}{\partial\theta} + \frac{1}{r}\left[\frac{\partial\hat{u}}{\partial z}\left(\frac{\partial\hat{u}}{\partial\theta} - \hat{v}\right) + \frac{\partial\hat{v}}{\partial z}\left(\frac{\partial\hat{v}}{\partial\theta} + \hat{u}\right) + \frac{\partial\hat{w}}{\partial\theta}\frac{\partial\hat{w}}{\partial z}\right], \tag{20d}$$

$$2\hat{\varepsilon}_{rz} = \frac{\partial\hat{w}}{\partial r} + \frac{\partial\hat{u}}{\partial z} + \frac{\partial\hat{u}}{\partial r}\frac{\partial\hat{u}}{\partial z} + \frac{\partial\hat{v}}{\partial r}\frac{\partial\hat{v}}{\partial z} + \frac{\partial\hat{w}}{\partial r}\frac{\partial\hat{w}}{\partial z}. \tag{20e}$$

The variational form of the plate kinetic energy is obtained from the following equation:

$$\delta K = \int_{-h/2}^{h/2}\int_0^{\theta_0}\int_{R_i}^{R_o} \rho\left(\frac{\partial u}{\partial t}\frac{\partial\delta u}{\partial t} + \frac{\partial v}{\partial t}\frac{\partial\delta v}{\partial t} + \frac{\partial w}{\partial t}\frac{\partial\delta w}{\partial t}\right) r\,\mathrm{d}r\,\mathrm{d}\theta\,\mathrm{d}z, \tag{21}$$

where $\rho[=\rho(z,T)]$ is the mass density of the FG plate.

Inserting Eqs. (17) and (19)–(21) into Eq. (18) and performing the integration by parts with respect to the spatial coordinate variables r, θ and temporal variable t, and also using the thermal equilibrium Eqs. (9) and (10), one obtains the equations of motion together with the related boundary conditions for small amplitude free vibration as follows:

δu:

$$\begin{aligned}&(\sigma_{0rr}+C_{11})\frac{\partial^2 u}{\partial r^2} + \left(\frac{C_{11}+\sigma_{0\theta\theta}}{r}\right)\frac{\partial u}{\partial r} + \left(\frac{\sigma_{0\theta\theta}+C_{44}}{r^2}\right)\frac{\partial^2 u}{\partial\theta^2} + (C_{44}+\sigma_{0zz})\frac{\partial^2 u}{\partial z^2} + 2\sigma_{0rz}\frac{\partial^2 u}{\partial r\,\partial z} + C'_{44}\frac{\partial u}{\partial z} - \left(\frac{\sigma_{0\theta\theta}+C_{11}}{r^2}\right)u\\ &- \left(\frac{2\sigma_{0\theta\theta}+C_{11}+C_{44}}{r^2}\right)\frac{\partial v}{\partial\theta} + \left(\frac{C_{44}+C_{12}}{r}\right)\frac{\partial^2 v}{\partial r\,\partial\theta} + (C_{44}+C_{12})\frac{\partial^2 w}{\partial r\,\partial z} + C'_{44}\frac{\partial w}{\partial r}\\ &= \rho\frac{\partial^2 u}{\partial t^2},\end{aligned} \tag{22}$$

δv:

$$\begin{aligned}&\left(\frac{2\sigma_{0\theta\theta}+C_{11}+C_{44}}{r^2}\right)\frac{\partial u}{\partial\theta} + \left(\frac{C_{12}+C_{44}}{r}\right)\frac{\partial^2 u}{\partial r\,\partial\theta} + (\sigma_{0rr}+C_{44})\frac{\partial^2 v}{\partial r^2} + \left(\frac{\sigma_{0\theta\theta}+C_{44}}{r}\right)\frac{\partial v}{\partial r} + \left(\frac{\sigma_{0\theta\theta}+C_{11}}{r^2}\right)\frac{\partial^2 v}{\partial\theta^2}\\ &+ (\sigma_{0zz}+C_{44})\frac{\partial^2 v}{\partial z^2} + 2\sigma_{0rz}\frac{\partial^2 v}{\partial r\,\partial z} + C'_{44}\frac{\partial v}{\partial z} - \left(\frac{\sigma_{0\theta\theta}+C_{44}}{r^2}\right)v + \left(\frac{C_{44}+C_{12}}{r}\right)\frac{\partial^2 w}{\partial z\,\partial\theta} + \left(\frac{C'_{44}}{r}\right)\frac{\partial w}{\partial\theta}\\ &= \rho\frac{\partial^2 v}{\partial t^2},\end{aligned} \tag{23}$$

δw:

$$C'_{12}\frac{\partial u}{\partial r}+(C_{12}+C_{44})\frac{\partial^2 u}{\partial z\,\partial r}+\left(\frac{C_{12}+C_{44}}{r}\right)\frac{\partial u}{\partial z}+\left(\frac{C'_{12}}{r}\right)u+\left(\frac{C_{12}+C_{44}}{r}\right)\frac{\partial^2 v}{\partial z\,\partial\theta}+\left(\frac{C'_{12}}{r}\right)\frac{\partial v}{\partial\theta}+(\sigma_{0rr}+C_{44})\frac{\partial^2 w}{\partial r^2}$$
$$+\left(\frac{\sigma_{0\theta\theta}+C_{44}}{r}\right)\frac{\partial w}{\partial r}+\left(\frac{\sigma_{0\theta\theta}+C_{44}}{r^2}\right)\frac{\partial^2 w}{\partial\theta^2}+(\sigma_{0zz}+C_{11})\frac{\partial^2 w}{\partial z^2}+2\sigma_{0rz}\frac{\partial^2 w}{\partial r\,\partial z}+C'_{11}\frac{\partial w}{\partial z}$$
$$=\rho\frac{\partial^2 w}{\partial t^2}. \tag{24}$$

The related boundary conditions become

At the surfaces $r=R_i$ and R_o:

$$\text{either } \delta u=0 \text{ or } (\sigma_{0rr}+C_{11})\frac{\partial u}{\partial r}+\sigma_{0rz}\frac{\partial u}{\partial z}+\left(\frac{C_{12}}{r}\right)u+\left(\frac{C_{12}}{r}\right)\frac{\partial v}{\partial\theta}+C_{12}\frac{\partial w}{\partial z}=0, \tag{25a, b}$$

$$\text{either } \delta v=0 \text{ or } \left(\frac{C_{44}}{r}\right)\left(\frac{\partial u}{\partial\theta}-v\right)+(\sigma_{0rr}+C_{44})\frac{\partial v}{\partial r}+\sigma_{0rz}\frac{\partial v}{\partial z}=0, \tag{26a, b}$$

$$\text{either } \delta w=0 \text{ or } C_{44}\frac{\partial u}{\partial z}+(\sigma_{0rr}+C_{44})\frac{\partial w}{\partial r}+\sigma_{0rz}\frac{\partial w}{\partial z}=0. \tag{27a, b}$$

At the surfaces $z=0$ and h:

$$\text{either } \delta u=0 \text{ or } (\sigma_{0zz}+C_{44})\frac{\partial u}{\partial z}+\sigma_{0rz}\frac{\partial u}{\partial r}+C_{44}\frac{\partial w}{\partial r}=0, \tag{28a, b}$$

$$\text{either } \delta v=0 \text{ or } \left(\frac{C_{44}}{r}\right)\frac{\partial w}{\partial\theta}+(\sigma_{0zz}+C_{44})\frac{\partial v}{\partial z}+\sigma_{0rz}\frac{\partial v}{\partial r}=0, \tag{29a, b}$$

$$\text{either } \delta w=0 \text{ or } C_{12}\frac{\partial u}{\partial r}+\left(\frac{C_{12}}{r}\right)u+\left(\frac{C_{12}}{r}\right)\frac{\partial v}{\partial\theta}+\sigma_{0rz}\frac{\partial w}{\partial r}+(C_{11}+\sigma_{0zz})\frac{\partial w}{\partial z}=0. \tag{30a, b}$$

3. Solution procedure

It is difficult to analytically solve the equations of motion, if it is not impossible. Hence, one should use an approximate method to find a solution. Here, the differential quadrature method (DQM) is employed. The basic idea of the differential quadrature method is that the derivative of a function, with respect to a space variable at a given sampling point, is approximated as a weighted linear sum of the sampling points in the domain of that variable. In order to illustrate the DQ approximation, consider a function $f(\xi,\eta)$ having its field on a rectangular domain $0\le\xi\le a$ and $0\le\eta\le b$. Let, in the given domain, the function values be known or desired on a grid of sampling points. According to DQ method, the rth derivative of the function $f(\xi,\eta)$ can be approximated as

$$\left.\frac{\partial^r f(\xi,\eta)}{\partial\xi^r}\right|_{(\xi,\eta)=(\xi_i,\eta_j)}=\sum_{m=1}^{N_\xi}A_{im}^{\xi(r)}f(\xi_m,\eta_j)=\sum_{m=1}^{N_\xi}A_{ij}^{\xi(r)}f_{mj}\quad\text{for } i=1,2,\ldots,N_\xi \text{ and } r=1,2,\ldots,N_\xi-1 \tag{31}$$

From this equation one can deduce that the important components of DQ approximations are the weighting coefficients ($A_{ij}^{\xi(r)}$) and the choice of sampling points. In order to determine the weighting coefficients a set of test functions should be used in Eq. (31). For polynomial basis functions DQ, a set of Lagrange polynomials are employed as the test functions. The weighting coefficients for the first-order derivatives in ξ_i-direction are thus determined as [20]

$$A_{ij}^{\xi}=\begin{cases}\dfrac{1}{a}\dfrac{M(\xi_i)}{(\xi_i-\xi_j)M(\xi_j)} & \text{for } i\neq j\\[2ex] -\displaystyle\sum_{\substack{j=1\\ i\neq j}}^{N_\xi}A_{ij}^{\xi} & \text{for } i=j\end{cases};\ i,j=1,2\ldots,N_\xi, \tag{32}$$

where $M(\xi_i)=\prod_{j=1,i\neq j}^{N_\xi}(\xi_i-\xi_j)$.

The weighting coefficients of the second-order derivative can be obtained as [20]

$$[B_{ij}^{\xi}]=[A_{ij}^{\xi}][A_{ij}^{\xi}]=[A_{ij}^{\xi}]^2. \tag{33}$$

In a similar manner, the weighting coefficients for the η-direction can be obtained.

A simple and natural choices of the grid distribution is the uniform grid spacing rule; however, it was found that non-uniform grid spacing yields results with better accuracy. Hence, in this study, the Chebyshev–Gauss–Lobatto quadrature

points are used, that is [20]

$$\frac{\xi_i}{a}=\frac{1}{2}\left\{1-\cos\left[\frac{(i-1)\pi}{(N_\xi-1)}\right]\right\},\frac{\eta_j}{b}=\frac{1}{2}\left\{1-\cos\left[\frac{(j-1)\pi}{(N_\eta-1)}\right]\right\}\text{for } i=1,2,\ldots,N_\xi;\ j=1,2,\ldots,N_\eta. \tag{34a, b}$$

Using the geometrical periodicity of the plate, the displacement components for the free vibration analysis can be represented as

$$u(r,\theta,z,t)=U_m(r,z)\mathrm{e}^{\mathrm{I}\omega_m t}\cos m\theta,\ v(r,\theta,z,t)=V_m(r,z)\mathrm{e}^{\mathrm{I}\omega_m t}\sin m\theta,\ w(r,\theta,z,t)=W_m(r,z)\mathrm{e}^{\mathrm{I}\omega_m t}\cos m\theta. \tag{35a–c}$$

where $m(=0,1,\ldots,\infty)$ is the circumferential wavenumber; ω_m is the natural frequency and $\mathrm{I}(=\sqrt{-1})$ is the imaginary number. It is obvious that $m=0$ means axisymmetric vibration.

At this stage the DQ rules are employed to discretize the free vibration equations and the related boundary conditions. Substituting for the displacement components from (35) and then using the DQ rules for the spatial derivatives, the discretized form of the equations of motion at each domain grid point (r_i,z_j) with $(i=2,3,\ldots,N_r-1)$ and $(j=2,3,\ldots,N_z-1)$ can be obtained as

Eq. (22):

$$\begin{aligned}&(\sigma_{0rr}+C_{11})_{ij}\sum_{n=1}^{N_r}B_{in}^{r}U_{mnj}+\frac{(C_{11}+\sigma_{0\theta\theta})_{ij}}{r_i}\Big(\sum_{n=1}^{N_r}A_{in}^{r}U_{mnj}\Big)+(C_{44}+\sigma_{0zz})_{ij}\sum_{k=1}^{N_z}B_{jk}^{z}U_{mik}\\&+2(\sigma_{0rz})_{ij}\sum_{n=1}^{N_r}\sum_{k=1}^{N_z}A_{in}^{r}A_{jk}^{z}U_{mnk}+(C'_{44})_{ij}\sum_{k=1}^{N_z}A_{jk}^{z}U_{mik}-[C_{11}+\sigma_{0\theta\theta}+m^2(C_{44}+\sigma_{0\theta\theta})]_{ij}\left(\frac{U_{mij}}{r_i^2}\right)\\&+\frac{m(C_{12}+C_{44})_{ij}}{r_i}\Big(\sum_{n=1}^{N_r}A_{in}^{r}V_{mnj}\Big)-m(C_{11}+C_{44}+2\sigma_{0\theta\theta})_{ij}\left(\frac{V_{mij}}{r_i^2}\right)+(C'_{44})_{ij}\sum_{n=1}^{N_r}A_{in}^{r}W_{mnj}\\&+(C_{12}+C_{44})_{ij}\sum_{n=1}^{N_r}\sum_{k=1}^{N_z}A_{in}^{r}A_{jk}^{z}W_{mnk}+\rho_{ij}\omega_m^2U_{mij}=0,\end{aligned} \tag{36}$$

Eq. (23):

$$\begin{aligned}&-\frac{m(C_{12}+C_{44})_{ij}}{r_i}\Big(\sum_{n=1}^{N_r}A_{in}^{r}U_{mnj}\Big)-m(2\sigma_{0\theta\theta}+C_{11}+C_{44})_{ij}\left(\frac{U_{mij}}{r_i^2}\right)+(\sigma_{0rr}+C_{44})_{ij}\sum_{n=1}^{N_r}B_{in}^{r}V_{mnj}\\&+\frac{(C_{44}+\sigma_{0\theta\theta})_{ij}}{r_i}\Big(\sum_{n=1}^{N_r}A_{in}^{r}V_{mnj}\Big)+(C_{44}+\sigma_{0zz})_{ij}\sum_{k=1}^{N_z}B_{jk}^{z}V_{mik}+(C'_{44})_{ij}\sum_{k=1}^{N_z}A_{jk}^{z}V_{mik}\\&+2(\sigma_{0rz})_{ij}\sum_{n=1}^{N_r}\sum_{k=1}^{N_z}A_{in}^{r}A_{jk}^{z}V_{mnk}-[m^2(C_{11}+\sigma_{0\theta\theta})+\sigma_{0\theta\theta}+C_{44}]_{ij}\left(\frac{V_{mij}}{r_i^2}\right)-m(C'_{44})_{ij}\left(\frac{W_{mij}}{r_i}\right)\\&-\frac{m(C_{44}+C_{12})_{ij}}{r_i}\Big(\sum_{k=1}^{N_z}A_{jk}^{z}W_{mik}\Big)+\rho_{ij}\omega_m^2V_{mij}=0,\end{aligned} \tag{37}$$

Eq. (24):

$$\begin{aligned}&(C'_{12})_{ij}\sum_{n=1}^{N_r}A_{in}^{r}U_{mnj}+\frac{(C_{12}+C_{44})_{ij}}{r_i}\sum_{k=1}^{N_z}A_{jk}^{z}U_{mik}+(C_{12}+C_{44})_{ij}\sum_{n=1}^{N_r}\sum_{k=1}^{N_z}A_{in}^{r}A_{jk}^{z}U_{mnk}\\&+(C'_{12})_{ij}\left(\frac{U_{mij}}{r_i}\right)+m(C'_{12})_{ij}\left(\frac{V_{mij}}{r_i}\right)+\frac{m(C_{12}+C_{44})_{ij}}{r_i}\Big(\sum_{n=1}^{N_z}A_{jk}^{z}V_{mik}\Big)+(\sigma_{0rr}+C_{44})_{ij}\sum_{n=1}^{N_r}B_{in}^{r}W_{mnj}\\&+\frac{(C_{44}+\sigma_{0\theta\theta})_{ij}}{r_i}\Big(\sum_{n=1}^{N_r}A_{in}^{r}W_{mnj}\Big)+2(\sigma_{0rz})_{ij}\sum_{n=1}^{N_r}\sum_{k=1}^{N_z}A_{in}^{r}A_{jk}^{z}W_{mnk}+(C_{11}+\sigma_{0zz})_{ij}\sum_{k=1}^{N_z}B_{jk}^{z}W_{mik}\\&+(C'_{11})_{ij}\sum_{k=1}^{N_z}A_{jk}^{z}W_{mik}-m^2(C_{44}+\sigma_{0\theta\theta})_{ij}\left(\frac{W_{mij}}{r_i^2}\right)+\rho_{ij}\omega_m^2W_{mij}=0.\end{aligned} \tag{38}$$

In a similar manner, at each boundary grid points, the boundary conditions can be discretized as follows:
Eq. (25):

$$\text{either } U_{mij}=0 \text{ or } (\sigma_{0rr}+C_{11})_{ij}\sum_{n=1}^{N_r}A_{in}^{r}U_{mnj}+\sum_{k=1}^{N_z}A_{jk}^{z}[(\sigma_{0rz})_{ij}U_{mik}+(C_{12})_{ij}W_{mik}]+(C_{12})_{ij}\left(\frac{U_{mij}+mV_{mij}}{r_i}\right)=0, \quad (39a, b)$$

Eq. (26):

$$\text{either } V_{mij}=0 \text{ or } -(C_{44})_{ij}\left(\frac{mU_{mij}+V_{mij}}{r_i}\right)+(C_{44}+\sigma_{0rr})_{ij}\sum_{n=1}^{N_r}A_{in}^{r}V_{mnj}+(\sigma_{0rz})_{ij}\sum_{k=1}^{N_z}A_{jk}^{z}V_{mik}=0, \quad (40a, b)$$

Eq. (27):

$$\text{either } W_{mij}=0 \text{ or } \sum_{k=1}^{N_z}A_{jk}^{z}[(C_{44})_{ij}U_{mik}+(\sigma_{0rz})_{ij}W_{mik}]+(\sigma_{0rr}+C_{44})_{ij}\sum_{n=1}^{N_r}A_{in}^{r}W_{mnj}=0, \quad (41a, b)$$

where i=1 and N_r at the surfaces $r=R_i$ and R_o, respectively.

Eq. (28):

$$\text{either } U_{mij}=0 \text{ or } (\sigma_{0zz}+C_{44})_{ij}\sum_{k=1}^{N_z}A_{jk}^{z}U_{mik}+\sum_{n=1}^{N_r}A_{in}^{r}[(\sigma_{0rz})_{ij}U_{mnj}+(C_{44})_{ij}W_{mnj}]=0, \quad (42a, b)$$

Eq. (29):

$$\text{either } V_{mij}=0 \text{ or } -m(C_{44})_{ij}\left(\frac{W_{mij}}{r_i}\right)+(C_{44}+\sigma_{0zz})_{ij}\sum_{k=1}^{N_z}A_{jk}^{z}V_{mik}+(\sigma_{0rz})_{ij}\sum_{n=1}^{N_r}A_{in}^{r}V_{mnj}=0, \quad (43a, b)$$

Eq. (30):

$$\text{either } W_{mij}=0 \text{ or } \sum_{n=1}^{N_r}A_{in}^{r}[(C_{12})_{ij}U_{mnj}+(\sigma_{0rz})_{ij}W_{mnj}]+(C_{12})_{ij}\left(\frac{U_{mij}+mV_{mij}}{r_i}\right)+(C_{11}+\sigma_{0zz})_{ij}\sum_{k=1}^{N_z}A_{jk}^{z}W_{mik}=0. \quad (44a, b)$$

where j=1 and N_z at the surfaces $z=0$ and h, respectively.

In order to carry out the eigenvalue analysis, the domain and boundary degrees of freedom should be separated. In vector forms, they are denoted as **d** and **b**, respectively. Based on these definitions, the DQ discretized form of the equations of motion and the related boundary conditions can be represented in the matrix form as

equations of motion:

$$\mathbf{S_{db}b}+\mathbf{S_{dd}d}-\omega_m^2\mathbf{Md}=\mathbf{0}, \quad (45)$$

boundary conditions:

$$\mathbf{S_{bb}b}+\mathbf{S_{bd}d}=\mathbf{0}. \quad (46)$$

The elements of the stiffness matrixes $\mathbf{S_{di}}$ (i=b, d) and the mass matrix **M** are obtained from equations of motion and those of the stiffness matrixes $\mathbf{S_{bi}}$ (i=b, d) are obtained from the boundary conditions.

Table 1
Temperature-dependent coefficients of material properties for ceramic (ZrO_2) and metals (Ti-6Al-4V).

	Material	Q_{-1}	Q_0	Q_1	Q_2	Q_3
E (GPa)	Ti-6A1-4V	0	122.7	-4.605×10^{-4}	0	0
	ZrO_2	0	132.2	-3.805×10^{-4}	-6.127×10^{-8}	0
v	Ti-6A1-4V	0	0.2888	1.108×10^{-4}	0	0
	ZrO_2	0	0.3330	0	0	0
$\rho\left(\frac{\text{kg}}{\text{m}^3}\right)$	Ti-6A1-4V	0	4420	0	0	0
	ZrO_2	0	3657	0	0	0
α (1/K)	Ti-6A1-4V	0	7.43×10^{-6}	7.483×10^{-4}	-3.621×10^{-7}	0
	ZrO_2	0	13.3×10^{-6}	-1.421×10^{-3}	9.549×10^{-7}	0
K (W/mK)	Ti-6A1-4V	0	6.10	0	0	0
	ZrO_2	0	1.78	0	0	0

Ref. [11].

Table 2
Convergence and accuracy of the first seven non-dimensional natural frequency parameters $\varpi_i[=\omega_{mi}h\sqrt{\rho/(C_{44})_m}]$ of clamped–clamped FG annular plates.

$N_r=N_z$	m	ϖ_1	ϖ_2	ϖ_3	ϖ_4	ϖ_5	ϖ_6	ϖ_7
7	0	8.177	13.912	15.516	19.446	20.108	21.720	22.552
9		8.201	13.875	15.511	19.481	20.158	21.888	22.615
13		8.209	13.870	15.511	19.485	20.164	21.885	22.615
19		8.210	13.870	15.511	19.486	20.165	21.885	22.615
3D_Ritz [17]		8.214	13.872	15.514	19.485	20.167	21.886	22.616
7	1	8.303	9.696	13.803	14.885	15.546	16.439	19.368
9		8.322	9.689	13.769	14.853	15.533	16.400	19.401
13		8.329	9.688	13.765	14.850	15.533	16.396	19.404
19		8.330	9.688	13.764	14.850	15.533	16.396	19.405
3D_Ritz [17]		8.333	9.689	13.766	14.850	15.535	16.397	19.404
7	2	8.849	11.160	13.842	15.638	16.561	17.684	19.326
9		8.861	11.147	13.814	15.615	16.548	17.628	19.365
13		8.865	11.145	13.810	15.614	16.549	17.623	19.368
19		8.866	11.144	13.810	15.614	16.549	17.623	19.369
3D_Ritz [17]		8.867	11.145	13.810	15.615	16.550	17.624	19.368

$R_i/R_o=0.4,\ h/R_o=0.5,\ \gamma=1,\ \Delta T=0.$

Table 3
Convergence and accuracy of the first seven non-dimensional natural frequency parameters $\varpi_i[=\omega_{mi}h\sqrt{\rho/(C_{44})_m}]$ of completely free FG annular plates.

$N_r=N_z$	m	ϖ_1	ϖ_2	ϖ_3	ϖ_4	ϖ_5	ϖ_6	ϖ_7
7	0	2.464	4.548	10.984	12.648	14.803	15.560	17.135
9		2.462	4.548	10.923	12.608	14.792	15.542	17.141
13		2.461	4.548	10.914	12.605	14.792	15.542	17.141
19		2.461	4.548	10.913	12.605	14.792	15.543	17.141
3D_Ritz [17]		2.461	4.549	10.910	12.602	14.788	15.538	17.136
7	1	3.655	5.120	10.842	11.072	11.632	12.474	14.523
9		3.653	5.119	10.795	11.042	11.596	12.440	14.502
13		3.652	5.119	10.788	11.038	11.591	12.437	14.500
19		3.652	5.119	10.788	11.038	11.590	12.437	14.500
3D_Ritz [17]		3.652	5.119	10.784	11.036	11.587	12.433	14.496
7	2	1.438	2.213	6.087	7.196	11.313	12.000	13.091
9		1.437	2.218	6.085	7.193	11.246	11.965	13.063
13		1.437	2.218	6.084	7.193	11.237	11.961	13.059
19		1.437	2.218	6.084	7.193	11.236	11.961	13.059
3D_Ritz [17]		1.437	2.219	6.084	7.192	11.233	11.959	13.056

$R_i/R_o=0.4,\ h/R_o=0.5,\ \gamma=1,\ \Delta T=0.$

Table 4
Convergence and accuracy of the first non-dimensional natural frequency parameter $[\omega_m h\sqrt{\rho_c/(C_{11})_c}]$ of clamped FG annular plates.

$N_r=N_z$	m	γ					
		0	1	2	3	4	5
7	0	0.199	0.195	0.184	0.168	0.150	0.132
9		0.199	0.195	0.184	0.169	0.152	0.135
13		0.199	0.195	0.184	0.169	0.152	0.135
3D_Ritz [17]		0.199	0.195	0.184	0.169	0.152	0.135
3D [16]		0.200	0.196	0.185	0.170	0.153	0.136
7	1	0.362	0.356	0.338	0.312	0.282	0.252
9		0.362	0.356	0.338	0.313	0.285	0.257
13		0.362	0.356	0.338	0.313	0.285	0.258
3D_Ritz [17]		0.363	0.356	0.338	0.313	0.285	0.258
3D [16]		0.368	0.361	0.343	0.318	0.289	0.261
7	2	0.532	0.523	0.499	0.464	0.423	0.381
9		0.532	0.523	0.499	0.465	0.427	0.389
13		0.532	0.523	0.499	0.465	0.427	0.389
3D_Ritz [17]		0.532	0.523	0.499	0.465	0.427	0.389
3D [16]		0.528	0.519	0.495	0.465	0.423	0.386

$h/R_o=0.3,\ \Delta T=0.$

Eliminating the boundary degrees of freedom from Eq. (45) using Eq. (46), the result reads

$$(\overline{\mathbf{S}} - \omega_m^2 \mathbf{M})\mathbf{D} = \mathbf{0}. \tag{47}$$

where $\overline{\mathbf{S}} = \mathbf{S_{dd}} - \mathbf{S_{db}}\mathbf{S_{bb}^{-1}}\mathbf{S_{bd}}$.

Solving the eigenvalue system of Eq. (47), the natural frequencies and mode shapes of the plate will be obtained.

4. Numerical results

In this section, firstly, the fast rate of convergence and high accuracy of the method is investigated. Then, the effects of the different geometrical parameters, the material parameters and the uniform and non-uniform temperature rise on the

Table 5
Convergence of the first three non-dimensional natural frequency parameters of FG annular plates subjected to non-uniform temperature rise.

$N_r = N_z$	m	C–C			F–C		
		λ_1	λ_2	λ_3	λ_1	λ_2	λ_3
7	0	54.718	126.756	176.049	10.619	62.735	98.532
9		54.533	125.433	175.967	9.249	65.523	96.607
13		54.449	125.275	175.873	12.735	59.769	99.586
15		54.433	125.248	175.856	12.691	59.839	99.522
17		54.424	125.233	175.846	12.673	59.860	99.497
19		54.419	125.224	175.841	12.666	59.866	99.487
FSDT		54.212	124.83	173.97	12.629	59.768	99.016
7	1	55.181	106.942	127.37	13.619	64.514	76.746
9		54.996	106.929	126.062	12.412	67.252	75.838
13		54.912	106.927	125.905	15.236	61.419	77.055
15		54.897	106.927	125.879	15.195	61.488	77.037
17		54.888	106.927	125.864	15.179	61.508	77.030
19		54.882	106.927	125.854	15.173	61.514	77.027
FSDT		54.677	107.19	125.45	15.157	61.433	76.869
7	2	56.709	121.239	129.244	20.591	69.622	83.801
9		56.526	121.216	127.979	19.616	71.617	82.153
13		56.445	121.207	127.825	21.553	66.254	84.646
15		56.430	121.205	127.800	21.517	66.319	84.600
17		56.421	121.204	127.785	21.504	66.337	84.582
19		56.416	121.204	127.776	21.499	66.343	84.574
FSDT		56.215	121.26	127.37	21.508	66.310	83.99

$R_i/R_o = 0.5,\ h/R_o = 0.1,\ p = 1,\ \Delta T = 800.$

Table 6
Convergence of the first three non-dimensional natural frequency parameters of FG annular plates subjected to non-uniform temperature rise.

$N_r = N_z$	m	C–C			F–C		
		λ_1	λ_2	λ_3	λ_1	λ_2	λ_3
7	0	38.387	77.929	88.293	11.866	43.583	49.932
9		38.372	77.921	88.195	11.894	43.595	49.922
13		38.346	77.906	88.15	11.884	43.571	49.927
19		38.337	77.899	88.136	11.881	43.561	49.927
FSDT		38.149	77.182	86.990	11.837	43.427	49.545
7	1	38.697	53.451	78.419	13.803	38.563	44.614
9		38.683	53.445	78.41	13.816	38.559	44.608
13		38.658	53.444	78.396	13.806	38.560	44.583
19		38.649	53.444	78.389	13.803	38.560	44.573
FSDT		38.460	53.578	77.669	13.789	38.427	44.451
7	2	39.790	60.601	79.892	18.727	42.379	47.693
9		39.779	60.587	79.879	18.721	42.37	47.641
13		39.757	60.583	79.865	18.711	42.373	47.614
19		39.749	60.582	79.859	18.709	42.373	47.604
FSDT		39.555	60.609	79.132	18.734	41.977	47.511

$R_i/R_o = 0.5,\ h/R_o = 0.2,\ p = 1,\ \Delta T = 800.$

free vibration characteristics of FG circular and annular plates are presented. Otherwise specified, the material properties vary according to power law distribution and the non-dimensional natural frequency parameters are defined as $\lambda_i = \omega_{mi} R_o^2 \sqrt{\rho_c h / D_{0c}}$, in which $D_{0c} = E_{0c} h^3 / 12(1 - \nu_{0c}^2)$. Also, the shear correction factor for the FSDT is assumed to be $\kappa = 5/(6 - \nu)$.

The material properties of Ti-6Al-4V and ZrO_2, as given in Table 1, are used in the numerical computations, which are chosen from the work of Kim [11]. They are valid for the temperature range of $300\,\mathrm{K} \leq T \leq 1100\,\mathrm{K}$.

As a first example, the convergence behavior and accuracy of the method for the first seven frequency parameters of thick FG annular plates with two different set of boundary conditions are studied in Tables 2 and 3. The results are compared with those of the three-dimensional elasticity solutions of Dong [17], which were obtained using the Chebyshev–Ritz method. The results for FG annular plates with both the inner and the outer surface clamped (C–C) are presented in Table 2 and for completely free FG annular plates (F–F) are given in Table 3. The material properties vary exponentially. The results are presented for different values of circumferential wavenumber (m). One can see that for each

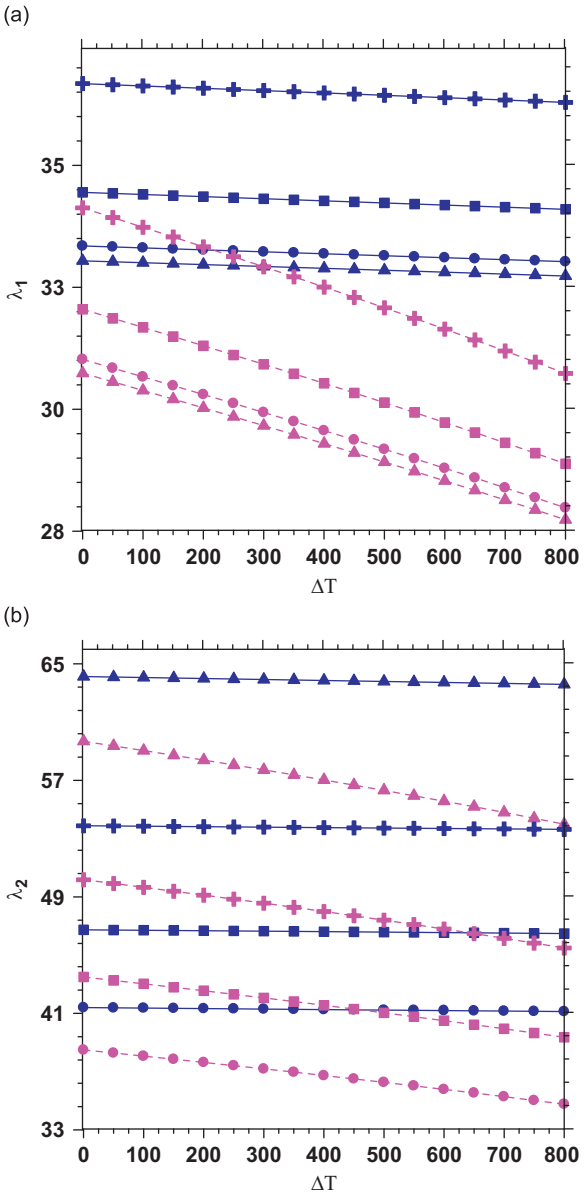

Fig. 2. (a)–(b). Comparison of the first two frequency parameters of the FG annular plates with and without the temperature-dependent material properties and subjected to non-uniform temperature rise ($h/R_o = 0.3$, $R_i/R_o = 0.5$, $p = 2$): ——— temperature independent, - - - - temperature dependent, ▲ m=0, ● m=1, ■ m=2, ✚ m=3.

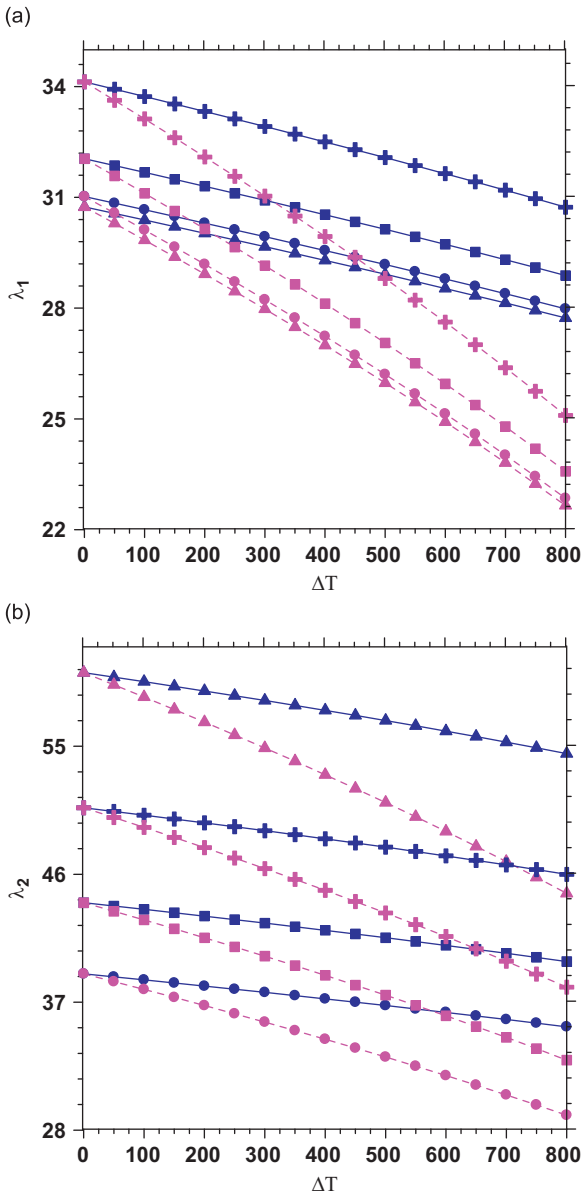

Fig. 3. (a)–(b). Comparison of the first two frequency parameters of the FG annular plates subjected to uniform and non-uniform temperature rise ($h/R_o = 0.3$, $R_i/R_o = 0.5$, $p = 2$): ——— non-uniform temperature rise, - - - - - uniform temperature rise, ▲ m=0, ● m=1, ■ m=2, ✚ m=3.

value of the circumferential wavenumber (m), the frequency parameters can be obtained accurately using only seven DQ grid points in each direction (r and z). Also, increasing the number of the grid points, the accuracy of the results increase without any numerical instability. It is evident that in all cases the results are in excellent agreement with those of the 3D elasticity theory.

As another example, the effect of the material property graded index (γ) on the convergence and accuracy of the first frequency parameter of clamped FG annular plates (C–C) are studied in Table 4. For the purposes of comparison, the results of the two other 3D approaches [16,17] are also cited. Again, the fast rate of convergence, numerical stability and accuracy of the method are quit obvious.

Since there are no available results for FG plate subjected to thermal environment, to validate the presented 3D approaches, the same problems are solved based on the FSDT. The convergence behavior of the presented 3D approach for the first three frequency parameters of moderately thick FG annular plates subjected to non-uniform temperature rise are presented in Tables 5 and 6. The results are calculated for two different values of the thickness-to-outer radius ratio and

also two different set of boundary conditions. In all cases, good agreement between the results of the two approaches, i.e. the 3D and the FSDT, are apparent.

After demonstrating the convergence and accuracy of the method, at this stage the effects of different parameters on the non-dimensional natural frequencies of the FG annular plates subjected to thermal environment are investigated.

In order to show the importance of considering the variation of material properties with temperature, the first two frequency parameters of the FG annular plates with and without the temperature-dependent material properties subjected to non-uniform temperature rise are compared in Figs. 2(a) and (b). The results are prepared for the different circumferential wavenumber (m). From these figures one can see that the frequency parameters are greatly overestimated when the temperature-dependence of material parameters is not taken into account. The discrepancy between temperature-dependent and temperature-independent solutions increase dramatically as the temperature rise increases.

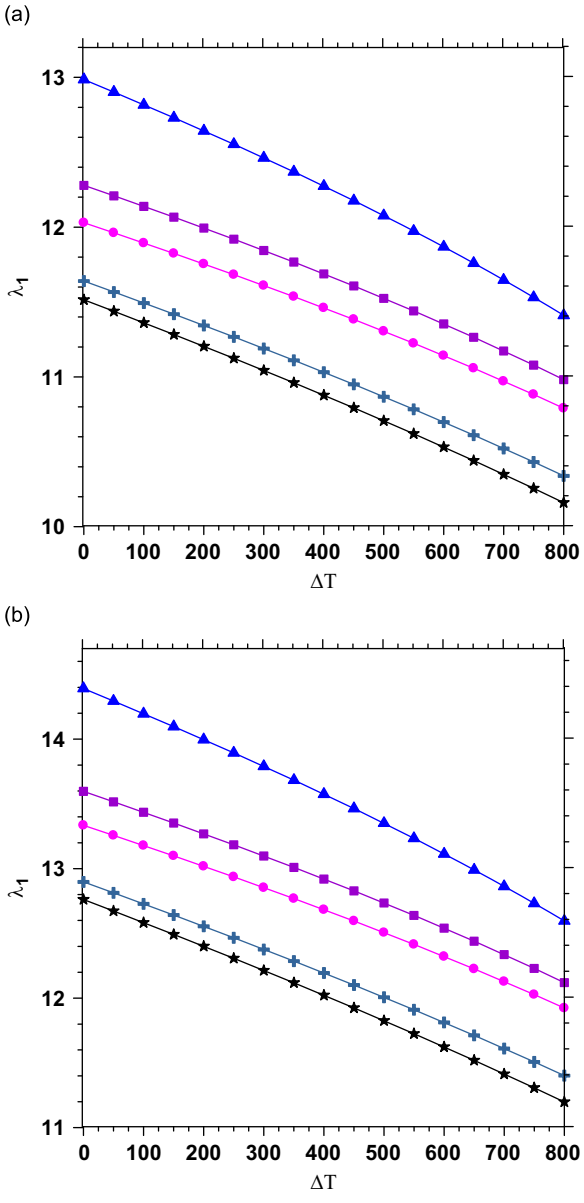

Fig. 4. The variation of the fundamental frequency parameters of the free-clamped FG annular plates against the temperature rise subjected to non-uniform temperature rise ($h/R_o = 0.3, R_i/R_o = 0.5$): p=0, p=0, p=1, p=5, p=10: (a) m=0 and (b) m=1.

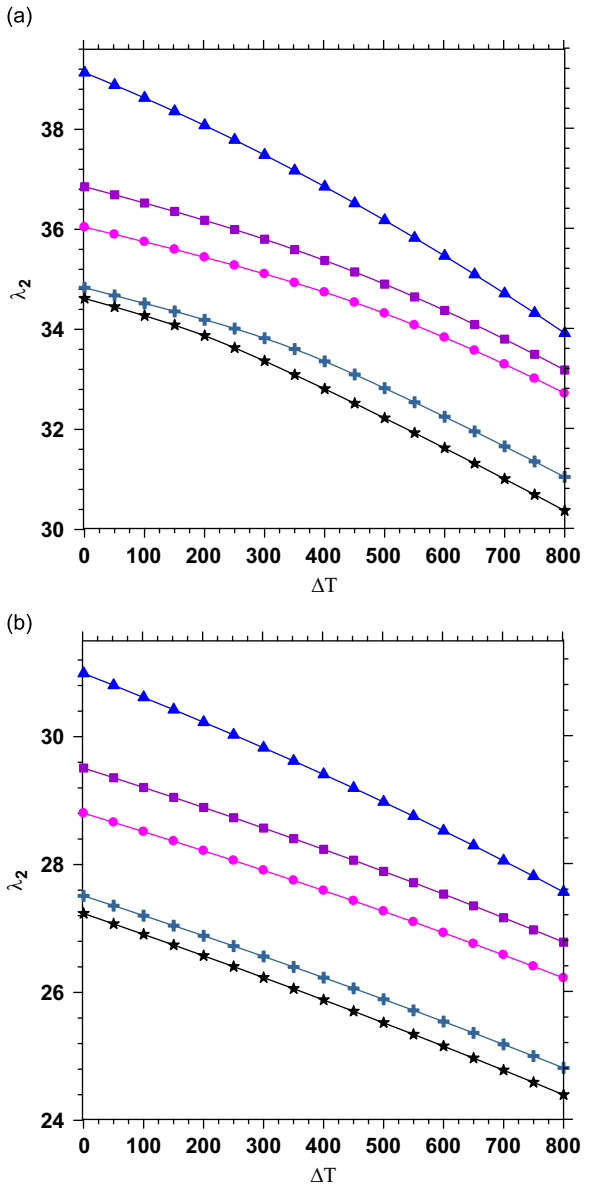

Fig. 5. The variation of the secondary frequency parameters of the free-clamped FG annular plates against the temperature rise subjected to non-uniform temperature rise ($h/R_o = 0.3, R_i/R_o = 0.5$): p=0, p=0, p=1, p=5, p=10: (a) m=0 and (b) m=1.

The influence of uniform and non-uniform temperature rise on the first three frequency parameters of FG annular plates are shown in Figs. 3(a) and (b). It can be seen that for the same value of temperature rise, the uniform temperature rise has more effect than non-uniform temperature rise on the frequency parameters and increasing the temperature rise, the discrepancy between the results of two cases increase dramatically.

The effects the non-uniform temperature rise on the first and the second frequency parameters of the FG annular plates with free inner edge and clamped outer edge (F–C) are presented in Figs. 4–5 for different values of the power law index (p). The results are shown for different values of the circumferential wavenumber (m). As obvious from these figures, increasing the temperature rise causes the frequency parameter to decrease monotonically for all values of the circumferential wavenumber (m).

In Table 7, the results for FG annular plates with two different values of inner-to-outer radius ratio, thickness-to-outer radius ratio and also two different sets of boundary conditions are presented. The influence of geometrical parameters and temperature rise on the first three non-dimensional natural frequency parameters of simply supported-clamped annular

Table 7
The influence of geometrical parameters on the first three non-dimensional natural frequency parameters of annular FG plate subjected to non-uniform temperature rise.

h/R_o	R_i/R_o	m	C–C			F–C		
			λ_1	λ_2	λ_3	λ_1	λ_2	λ_3
0.1	0.1	0	18.438	47.537	86.074	6.617	26.777	58.661
		1	19.230	49.487	68.801	14.382	39.535	54.399
		2	24.528	57.151	85.543	23.462	54.310	76.854
	0.3	0	30.006	73.998	129.169	7.633	35.165	81.611
		1	30.695	75.064	82.589	12.918	39.318	62.055
		2	33.331	78.459	99.928	22.035	50.377	69.061
0.2	0.1	0	15.470	35.349	54.009	6.907	23.334	45.183
		1	16.417	34.455	37.364	13.447	27.228	31.949
		2	21.215	42.833	43.560	20.632	38.466	42.222
	0.3	0	23.603	50.922	64.733	7.782	28.717	43.345
		1	24.145	41.308	51.791	12.044	31.013	31.406
		2	26.333	50.19	54.467	19.483	34.54	38.803

$\Delta T = 800$, $p = 1$.

Table 8
The influence of geometrical parameters and temperature rise on the first three non-dimensional natural frequency parameters of simply supported-clamped annular FG plate subjected to non-uniform temperature rise.

h/R_o	R_i/R_o	m	$\Delta T = 200$			$\Delta T = 800$		
			λ_1	λ_2	λ_3	λ_1	λ_2	λ_3
0.1	0.1	0	17.754	48.106	89.629	15.667	43.293	81.439
		1	19.698	51.608	72.191	17.258	46.436	66.958
		2	27.348	62.330	91.046	24.081	56.177	84.433
	0.3	0	26.183	72.734	93.470	23.551	66.240	86.735
		1	27.715	74.455	87.385	24.874	67.794	81.072
		2	32.600	79.641	102.03	29.175	72.491	94.677
0.2	0.1	0	15.357	37.150	53.397	13.964	34.028	49.568
		1	17.090	36.159	39.815	15.504	33.538	36.460
		2	23.195	45.590	47.277	21.076	42.278	43.320
	0.3	0	21.918	46.862	52.905	20.055	43.488	48.705
		1	23.074	43.748	50.371	21.098	40.586	46.680
		2	26.741	51.103	57.429	24.431	47.423	52.855

$p = 1$.

FG plate subjected to non-uniform temperature rise are presented in Table 8. The plates are subjected to non-uniform temperature rise.

The effects of the thickness-to-outer radius ratio on the frequency parameters of the clamped FG annular plates subjected to the thermal environment and for the various inner-to-outer radius ratio are shown in Fig. 6. As one can see, increasing the thickness-to-outer radius ratio causes the frequency parameters to decrease. This is due to definition of the non-dimensional frequency parameters. But, it should be noted that the frequency ω_{mi} increases by increasing this ratio. Also, one can see that the frequency parameters can be highly nonlinear, when compared with the cases in other figures, which represent the effects of other parameters.

The mode shapes of the FG annular plates with free inner edge and clamped outer edge (F–C) in thermal environment are shown in Fig. 7. From Fig. 7, it can be seen that the displacement modes of the first frequency parameter are axisymmetric and those of the other frequency parameters are asymmetric. It should be mentioned that increasing the temperature rise or the power law index (p), the mode shapes have not significant changes in shape.

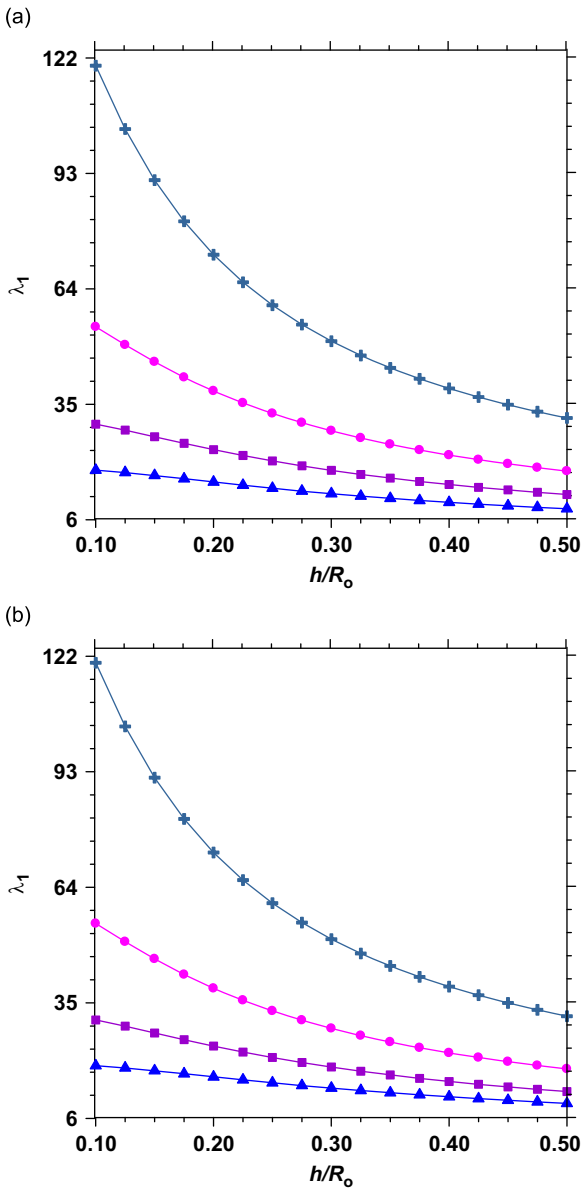

Fig. 6. The influence of the thickness-to-outer radius ratio on the frequency parameters of the clamped FG annular plates ($\Delta T = 800\,\mathrm{K}$, $p = 1$): $R_i/R_o = 0.1$, $R_i/R_o = 0.3$, $R_i/R_o = 0.5$, $R_i/R_o = 0.7$: (a) m=0 and (b) m=1.

5. Conclusion

The three-dimensional free vibration analysis of thick FG annular plates subjected to thermal environment is presented. The material properties are assumed to be temperature dependent and graded in the thickness direction. The initial thermal stresses are obtained by solving the equilibrium equations of the plate. Using Hamilton's principle, the equations of motion and the related boundary conditions subjected to initial thermal stresses are derived. The differential quadrature method as an efficient and accurate numerical tool is used to solve the system of equilibrium equations and equations of motion. Using the DQ method, allows one to deal with FG plates with an arbitrary thickness distribution of material properties and also to implement the boundary conditions of the plate efficiently and in an exact manner. The convergence behavior and accuracy of the method are investigated through the different solved examples. The effects of the temperature rise, the geometrical parameters and the material graded index on the frequency parameters are investigated. It is shown that the temperature-dependence of the material properties have significant effects on the natural frequency parameters. Also, increasing the temperature rise, the natural frequencies decrease. It

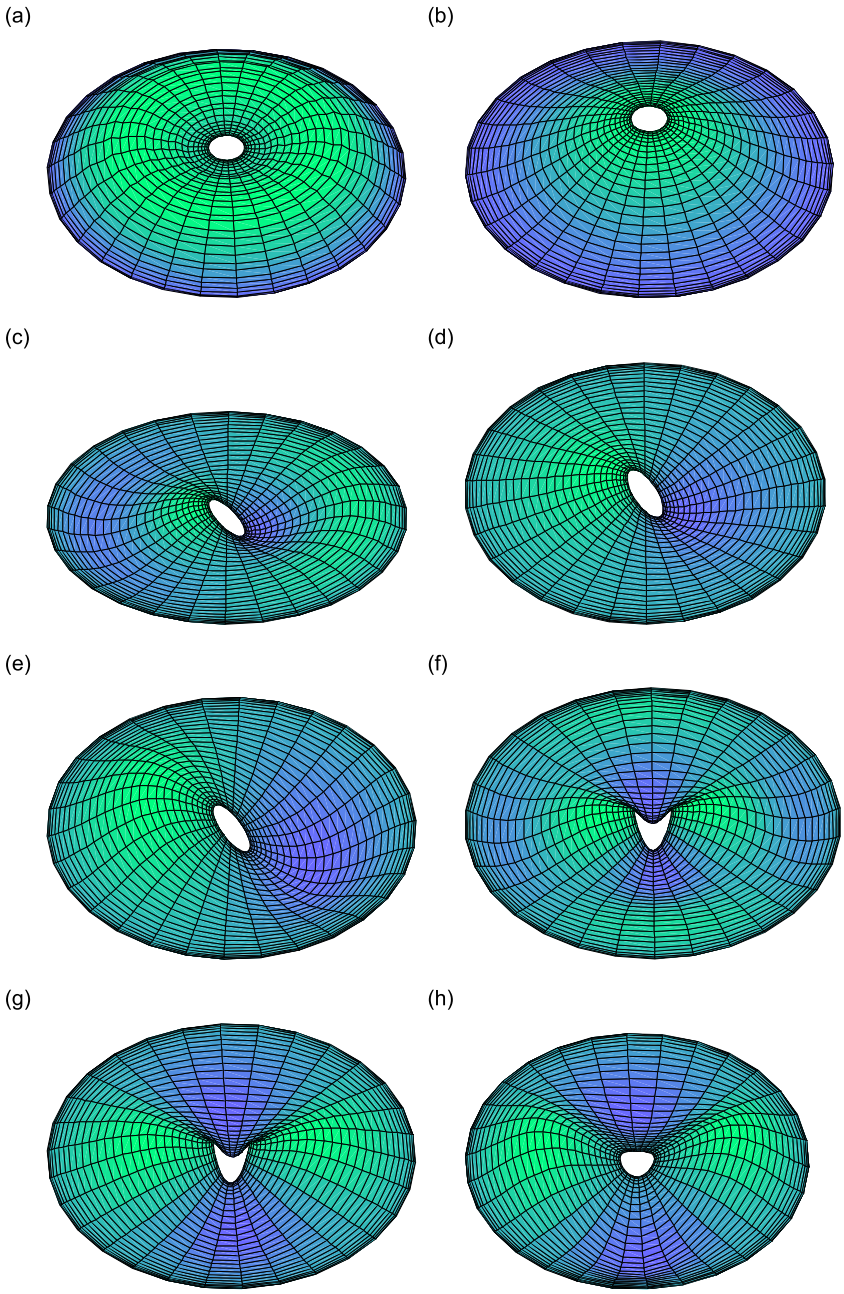

Fig. 7. The displacement modes of the free-clamped FG annular plates ($\Delta T = 800\,\mathrm{K}$, $R_i/R_o = 0.1$, $h/R_o = 0.3$, $p = 1$): (a) m=0, the radial displacement (u), (b) m=0, the transverse displacement (w), (c) m=1, the radial displacement (u), (d) m=1, the tangential displacement (v), (e) m=1, the transverse displacement (w), (f) m=2, the radial displacement (u), (g) m=2, the tangential displacement (v) and (h) m=2, the transverse displacement (w).

should be mentioned that increasing the temperature rise or the power law index (p), the mode shapes have no significant changes in shape. The new tabulated results can be used as benchmark for other numerical methods and also the refined plate theories.

References

[1] M. Aydogdu, V. Taskin, Free vibration analysis of functionally graded beams with simply supported edges, *Material and Design* 28 (2007) 1651–1656.
[2] S.A. Fazelzadeh, P. Malekzadeh, P. Zahedinejad, M. Hosseini, Vibration analysis of functionally graded thin-walled rotating blades under high temperature supersonic flow using the differential quadrature method, *Journal of Sound and Vibration* 306 (2007) 333–348.

[3] H.J. Xiang, J. Yang, Free and forced vibration of a laminated FGM Timoshenko beam of variable thickness under heat conduction, *Composites: Part B* 39 (2008) 292–303.
[4] S.C. Pradhan, T. Murmu, Thermo-mechanical vibration of FGM sandwich beam under variable elastic foundations using differential quadrature method, *Journal of Sound and Vibration* 282 (2008) 509–516.
[5] M.T. Piovan, R. Sampaio, Vibrations of axially moving flexible beams made of functionally graded materials, *Thin-Walled Structures* 46 (2008) 112–121.
[6] C.S. Chen, T.J. Chen, R.D. Chien, Nonlinear vibration of initially stressed functionally graded plates, *Thin-Walled Structures* 44 (2006) 844–851.
[7] R.C. Batra, J. Jin, Natural frequencies of a functionally graded anisotropic rectangular plate, *Journal of Sound and Vibration* 282 (2005) 509–516.
[8] J. Yang, H.S. Shen, Vibration characteristics and transient response of shear-deformable functionally graded plates in thermal environment, *Journal of Sound and Vibration* 255 (2002) 579–602.
[9] L.F. Qian, R.C. Batra, L.M. Chen, Static and dynamic deformations of thick functionally graded elastic plates by using higher-order shear and normal deformable plate theory and meshless local Petrov–Galerkin method, *Composites: Part B* 35 (2004) 685–697.
[10] R.C. Batra, Higher-order shear and normal deformable theory for functionally graded incompressible linear elastic plates, *Thin-Walled Structures* 45 (2007) 974–982.
[11] Y.W. Kim, Temperature dependent vibration analysis of functionally graded rectangular plates, *Journal of Sound and Vibration* 284 (2005) 531–549.
[12] P. Malekzadeh, Three-dimensional free vibration analysis of thick functionally graded plates on elastic foundations, *Composite Structures* 89 (2009) 367–373.
[13] A.N. Eraslan, T. Akis, On the plane strain and plane stress solutions of functionally graded rotating solid shaft and solid disk problems, *Acta Mechanica* 181 (2006) 43–63.
[14] T. Prakash, M. Ganapathi, Asymmetric flexural vibration and thermoelastic stability of FGM circular plates using finite element method, *Composites: Part B* 37 (2006) 642–649.
[15] E. Efraim, M. Eisenberger, Exact vibration analysis of variable thickness thick annular isotropic and FGM plates, *Journal of Sound and Vibration* 299 (2007) 720–738.
[16] G.J. Nie, Z. Zhong, Semi-analytical solution for three-dimensional vibration of functionally graded circular plates, *Computer Methods in Applied Mechanics and Engineering* 196 (2007) 4901–4910.
[17] C.Y. Dong, Three-dimensional free vibration analysis of functionally graded annular plates using the Chebyshev–Ritz method, *Materials and Design* 29 (2008) 1518–1525.
[18] X. Zhao, Y.Y. Lee, K.M. Liew, Free vibration analysis of functionally graded plates using the element-free kp-Ritz method, *Journal of Sound and Vibration* 319 (2009) 918–939.
[19] B.R. Kumar, N. Ganesan, R. Sethuraman, Vibro-acoustic analysis of functionally graded elliptic disc under thermal environment, *Mechanics of Advanced Materials and Structures* 16 (2009) 160–172.
[20] C.W. Bert, M. Malik, Differential quadrature method in computational mechanics: Aa review, *Applied Mechanics Review* 49 (1996) 1–27.
[21] P. Malekzadeh, Differential quadrature large amplitude free vibration analysis of laminated skew plates based on FSDT, *Composite Structures* 83 (2008) 189–200.
[22] P. Malekzadeh, A.R. Setoodeh, E. Barmshouri, A hybrid layerwise and differential quadrature method for in-plane free vibration of laminated thick circular arches, *Journal of Sound and Vibration* 315 (2008) 215–225.
[23] P. Malekzadeh, Nonlinear free vibration of tapered Mindlin plates with edges elastically restrained against rotation using DQM, *Thin-Walled Structures* 46 (2008) 11–26.